REPORT DOCUMENTATION PAGE	Form Approved OMB NO. 0704-0188

1. REPORT DATE (DD-MM-YYYY) 20-12-2018	2. REPORT TYPE Final Report	3. DATES COVERED (From - To) 1-Sep-2015 - 31-Aug-2018

4. TITLE AND SUBTITLE Final Report: Numerical Simulation of Atmospheric Boundary Layer Flow over Battle Eld-Scale Complex Terrain: Surface Fluxes from Resolved	5a. CONTRACT NUMBER W911NF-15-1-0231
	5b. GRANT NUMBER
	5c. PROGRAM ELEMENT NUMBER 611102
6. AUTHORS	5d. PROJECT NUMBER
	5e. TASK NUMBER
	5f. WORK UNIT NUMBER

7. PERFORMING ORGANIZATION NAMES AND ADDRESSES University of Texas at Dallas 800 West Campbell Road, AD15 Richardson, TX 75080 -3021	8. PERFORMING ORGANIZATION REPORT NUMBER
9. SPONSORING/MONITORING AGENCY NAME(S) AND ADDRESS (ES) U.S. Army Research Office P.O. Box 12211 Research Triangle Park, NC 27709-2211	10. SPONSOR/MONITOR'S ACRONYM(S) ARO 11. SPONSOR/MONITOR'S REPORT NUMBER(S) 65843-CH.1

12. DISTRIBUTION AVAILIBILITY STATEMENT

Approved for public release; distribution is unlimited.

13. SUPPLEMENTARY NOTES

The views, opinions and/or findings contained in this report are those of the author(s) and should not contrued as an official Department of the Army position, policy or decision, unless so designated by other documentation.

14. ABSTRACT

15. SUBJECT TERMS

16. SECURITY CLASSIFICATION OF: a. REPORT	b. ABSTRACT	c. THIS PAGE	17. LIMITATION OF ABSTRACT	15. NUMBER OF PAGES	19a. NAME OF RESPONSIBLE PERSON
UU	UU	UU	UU		William Anderson
					19b. TELEPHONE NUMBER 972-883-4660

Standard Form 298 (Rev 8/98)
Prescribed by ANSI Std. Z39.18

RPPR Final Report
as of 02-Jan-2019

Agency Code:

Proposal Number: 65843CH **Agreement Number: W911NF-15-1-0231**

INVESTIGATOR(S):

Name: Ph.D. William Anderson
Email: william.anderson@utdallas.edu
Phone Number: 9728834660
Principal: Y

Organization: **University of Texas at Dallas**
Address: 800 West Campbell Road, AD15, Richardson, TX 750803021
Country: USA
DUNS Number: 800188161 EIN: 751305566
Report Date: 30-Nov-2018 Date Received: 20-Dec-2018
Final Report for Period Beginning 01-Sep-2015 and Ending 31-Aug-2018
Title: Numerical Simulation of Atmospheric Boundary Layer Flow over Battle Eld-Scale Complex Terrain: Surface Fluxes from Resolved
Begin Performance Period: 01-Sep-2015 **End Performance Period:** 31-Aug-2018
Report Term: 0-Other
Submitted By: Ph.D. William Anderson Email: william.anderson@utdallas.edu
Phone: (972) 883-4660
Distribution Statement: 1-Approved for public release; distribution is unlimited.

STEM Degrees: **STEM Participants:**

Major Goals: Please see attached narrative.

Accomplishments: Please see attached narrative.

Training Opportunities: Nothing to Report

Results Dissemination: Please see attached narrative.

Honors and Awards: PI received tenure and was recipient of endowed professorship (Eugene McDermott Professor) during research effort. This professorship is designed to promote high risk, high reward, discretionary research efforts, and receipt is based upon prior research productivity. In this sense, ARO support contributed positively towards the PI's overall nomination for the professorship.

Protocol Activity Status:

Technology Transfer: Nothing to Report

PARTICIPANTS:

Participant Type: PD/PI
Participant: William Anderson
Person Months Worked: 1.00 **Funding Support:**
Project Contribution:
International Collaboration:
International Travel:
National Academy Member: N
Other Collaborators:

RPPR Final Report
as of 02-Jan-2019

THE UNIVERSITY OF TEXAS AT DALLAS

Annual Report for Grant # W911NF-15-1-0231, Project # 65843-CH

Numerical simulation of atmospheric boundary-layer flow over battlefield-scale complex terrain: surface fluxes from resolved and subgrid scales

A final report submitted to the Army Research Office, Environmental Chemistry Program
(Program Manager: Dr. Robert A. Mantz)

PI: William Anderson, Mechanical Engineering Department, The University of Texas at Dallas

1. Background

The atmospheric boundary layer (ABL) – the dense, thin layer of the atmosphere nearest to the Earth – is dominated by vigorous turbulent mixing produced by aerodynamic drag (shear) and thermal forcing (buoyancy). The depth of the ABL, H, varies with the diurnal cycle, where radiative surface heating during daytime hours acts in conjunction with ambient shear to thicken the ABL, while during nighttime hours the relatively cool surface reverses the affect of buoyancy and suppresses the production of turbulence via shear. The relative contribution to turbulence production via shear and buoyancy is commonly quantified via the Obukhov length. In the absence of buoyancy (neutral conditions), turbulence is produced only via shear. For conceptual purposes, the neutrally-stratified ABL may be divided vertically into two horizontal layers: the surface and inertial layer, where the former occupies the lowest ≈ 10 % of the ABL and is heavily influenced by attributes of the underlying landscape, while the latter is presumed to be horizontally homogeneous for a "balanced" ABL [1] and is affected by Coriolis accelerations. This vertical layering can be defined with the profiles [2]:

$$\frac{\langle u(z)\rangle_{xyt}}{u_*} = \frac{1}{\kappa}\ln\left(\frac{z-d}{z_0}\right), \tag{1}$$

and

$$\frac{\langle u(z)\rangle_{xyt} - U_G}{u_*} = \frac{1}{\kappa}\ln\left(\frac{zf}{u_*}\right) + C, \tag{2}$$

where, in this report, the first, second, and third components of any vector correspond with the streamwise, spanwise, and vertical component, respectively (i.e., $\boldsymbol{x} = x\hat{i} + y\hat{j} + z\hat{k}$). Moreover, averaging over dimension, a, is denoted by $\langle ... \rangle_a$. Equation 1, thus, defines mean (Reynolds averaged) streamwise wind in the surface layer, while Equation 2 defines the tendency of $\langle u(z)\rangle_{xyt}$ towards the outer flow associated with the geostrophic balance (i.e., $U_G = -\left(f\rho\right)^{-1} \mathrm{d}p_0/\mathrm{d}x$, where f is the Coriolis parameter, ρ is atmospheric density, and $\mathrm{d}p_0/\mathrm{d}x$ is the aloft pressure gradient). In Equations 1 and 2, $u_* = (\tau_w/\rho)^{1/2} = [(H/\rho)\,\mathrm{d}p_0/\mathrm{d}x]^{1/2}$. In Equation 2, the additive constant is $C \approx 4.3$ [2], while in Equation 1, z_0 is the elevation at which $\langle u(z)\rangle_{xyt} = 0$, otherwise known as the momentum roughness length, and d is displacement height [3, 4]. The Project # 65843-CH research effort is directed towards development of prognostic models for z_0 in Equation 1 – especially for complex, multiscale topographies that exhibit self similarity over a broad spectrum of modes (whether associated with fractal landscapes [5, 6], vegetative canopies [7], urban geometries [8], or simply with understanding how turbulent shear flows respond to canonical fractal geometries [9, 10]). Since z_0 is the only input argument required to define $\langle u(z)\rangle_{xyt}$, its importance to numerical weather prediction at battlefield scales cannot be overstated.

Consider, for example, atmospheric flow over a representative urban landscape, $h(x,y)$. The smallest scale at which $h(x,y)$ exhibits variability, δ_R, is expected to be $\delta_R \sim 10^{-1}$ m. In large-eddy simulations (LES) of the atmospheric boundary layer, where the computational domain extent is $L \sim 10^3$ m, the number of grid points, N, sets the computational resolution, δ_C. In recent times, atmospheric LES with $N \sim 10^3$ have been performed [11, 12], although these incur an immense computational challenge, and in reality $N \sim 10^2$ is more widespread. With this, one can deduce that the computational mesh resolution, δ_C, is typically $\delta_C \sim 10^0$ to 10^1 m, and thus $R \sim \delta_R/\delta_C \gtrsim 10^1$. ***This rudimentary deduction highlights the challenges inherent to modeling atmospheric surface layer turbulence over complex, natural terrains, and motivate the need for prognostic wall models.***

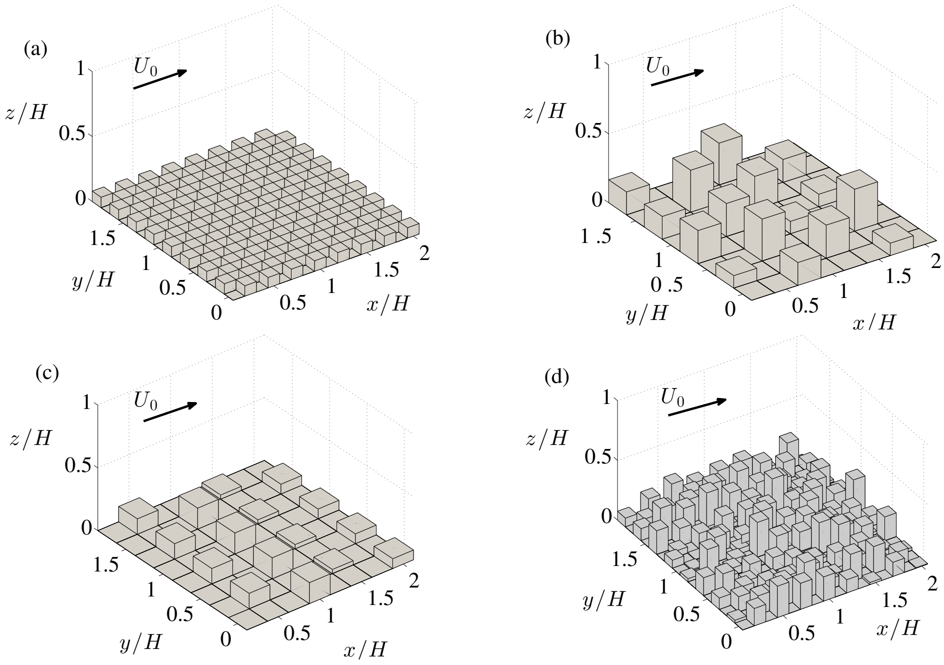

Figure 1: Illustration of synthetic, urban-like topographies considered in Zhu et al. [13] with freestream flow, U_0, added to denote forcing direction. Panel (a) shows a uniform height arrangement, Panels (b) and (c) show cases with bimodal heights, and Panel (c) shows a random case.

Given the physical definition of z_0 (embodied in Eq. 1), it follows that a unique z_0 exists for each topography. z_0 can be found *a posteriori* via experimental measurement, whereby the Reynolds-averaged velocity profile is used to infer z_0. The practical limitations on this approach are obvious, and this has motivated development of prognostic models. *A priori* estimation of z_0 based only on geometric details of the topography is an open research effort in boundary-layer meteorology. Models for z_0 play an important role in numerical weather prediction and generating realistic inflow conditions for simulations of ABL turbulence [14–16].

During the Year # 1 research effort, we showed that models for z_0 and d derived from the "engineering approach" can be leveraged in boundary-layer meteorology approaches [13, 16, 17]. Specifically, we showed that:

$$d = d(\sigma_h) = \alpha_d \sigma_h, \tag{3}$$

where $\alpha_d = 1.69$, and σ_h is root-mean-square height, and

$$z_0(\sigma_h, sk) = \begin{cases} \alpha_G \sigma_h (1 + \beta sk), & \sigma_h/\langle h\rangle_{xy} + z_{0,p} < 1.15 \\ \alpha_G \sigma_h (1 + sk)^{\beta}, & \sigma_h/\langle h\rangle_{xy} + z_{0,p} \geq 2. \end{cases} \tag{4}$$

In Equation 4, $\beta = 0.9$, $\alpha_G = 0.1$, $z_{0,p}$ is a "base" aerodynamic roughness to capture the influence of small-scale elements, and s_k is the skewness of $h(x, y)$. In Zhu et al. [13], the efficacy of Eq. 4 was rigorously assessed via a comprehensive parametric study, all of which confirmed that: (1) skewness is an important topographic momentum in setting the momentum roughness length; and (2) only root-mean-square height is needed to model displacement height. Figure 1 illustrates sample cases considered for the parametric testing. But, the cases considered in Zhu et al. [13] were "fully resolved", i.e., $R = 1$. During the final years of the research effort, we considered fractal cities with $R > 1$, and leveraged the prognostic capabilities of Equations 3 and 4 to predict "subgrid-scale height" effects.

2. Urban Fractal Geometries

In this study, we consider urban-like fractal geometries constructed via iterated function systems (IFS) [18]. An IFS topology is, by definition, fractal, and is built via successive inner product computations, $\{f_i : \mathcal{X} \to \mathcal{X} | i = 1, 2, \ldots, N_g\}$, where $\mathcal{X}$ is the underlying vector space. The resultant function, $\mathcal{F} = (\mathcal{X} : f_1, f_2, ..., f_M)$, is an IFS. For the present cases, we define f_i such that the side length and height of each successive generation is $l_{g+1} = rl_g$ and $h_{g+1} = rh_g$, where r is a predefined scale-reduction factor. In order to consider topographies based upon a self-similar, Sierpiński carpet template, we necessarily adopt $r = 1/3$ for all cases (values exceeding this are not possible, while values less than this would result in highly skewed topographies that would present resolution challenges and not resemble urban-like topographies). In order to consider more realistic cases, we added a random horizontal displacement to each successive mapping, such that the blocks were self-similar across generations but displaced laterally to promote randomness. Figure 2 shows a sample fractal city, built with IFS.

By virtue of the IFS approach, fractal dimension is nominated *a priori* via $D = \log(N_b)/\log(r^{-1})$, where N_b is the repeating factor (the number of descendant elements added during each IFS iteration). Since the present topographies are composed via superposition of self-similar blocks, the spectral density of height will not exhibit a power law dependence on wavelength with spectral exponent, β_s (unlike the landscapes considered by [6]). Instead, the spectral density of the skewed topographies would feature distinct peaks across the range of constituent wavelengths. Thus, Orey's formula may not be used to relate spectral exponent and fractal dimension. In total, we consider 33 cases in this article, where Case 1 is a surface without any blocks, and serves the role of a benchmark case against which others are compared. In the IFS construction process, the first generation is a single block at the geometric center (Case 2; Figure 2a); beyond this, we consider the five series with different fractal dimension, D, and increasing number of generations, N_g (Figure 2b-d). Cases 18 to 22 are identical to Case 2, but with an added drag for sub-generation elements (defined via the equilibrium logarithmic law, where effective roughness length is defined with Equation 4).

To assess the role of the random spatial shift added during each successive generation for Cases 3 to 17, we have also modeled flow over Cases 23 to 28, which are "pure" Sierpiński carpet topographies with no spatial shift. Cases 23 to 25 are built with $D = 1.2619$ (i.e., a comparison against Cases 3 to 5), while Cases 26 to 27 are built with $D = 1.8928$ (i.e., a comparison against Cases 15 to 17). Finally, as a matter of completeness, results of grid-sensitivity testing are presented in Appendix A. Cases 29, 30, 31, 32, and 33 are geometrically identical to Cases 5, 8, 11, 14, and 17, respectively, but the simulations have been carried out at higher resolution. Results have indicated no sensitivity between the high- and low-resolution cases.

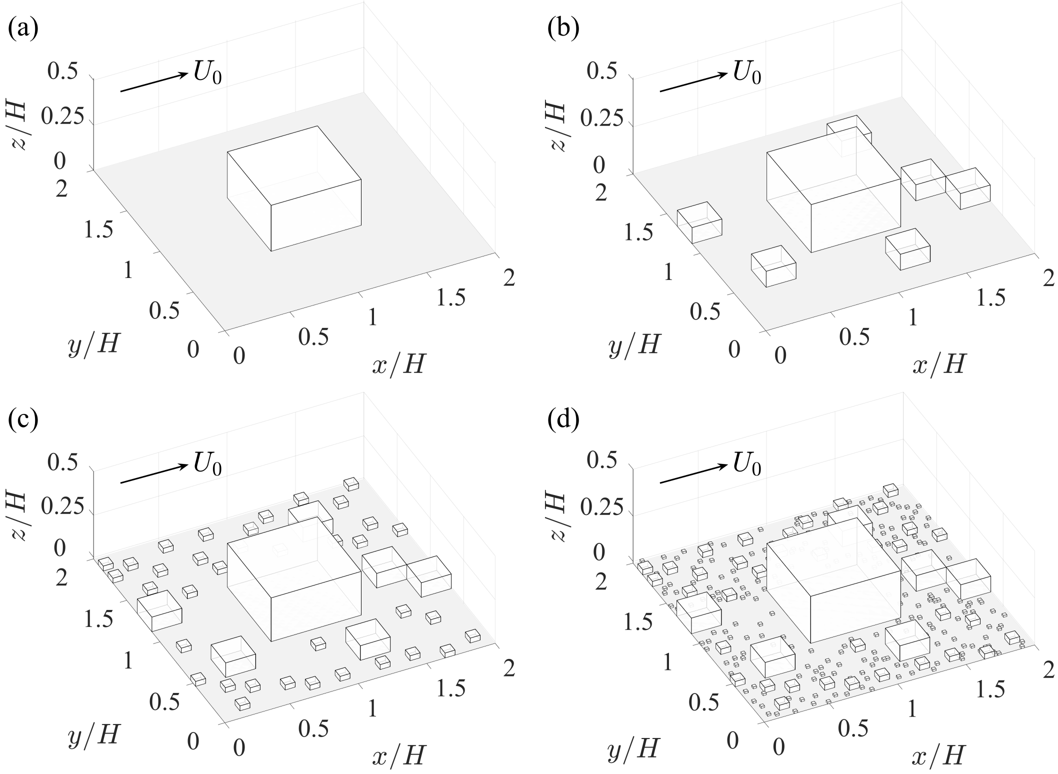

Figure 2: Illustration of multiscale, fractal-like urban topographies of Series 3 ($D = 1.6309$): Panels (a) to (d) show Case 2, Case 9, Case 10, and Case 11, respectively. The topographies built in this figure are based on the Sierpiński carpet template with random horizontal shift, so they are fractals with self-similarity among generations. For example, in Panel (b), the six descendant blocks are self similar with the large central block in Panel (a), with the relation: $l_2 = r \times l_1$ and $h_2 = r \times h_1$, where $r = 1/3$ is the scale-reduction factor. Annotation, U_0, added to denote streamwise forcing direction.

Case	Series	N_b	D	N_g	$(\hat{z}_0/H)^*$	d/H	$z_{0,\mathrm{Eff.}}/H^*$	$\alpha_g(N_g, D)$	$\alpha(D)$
1	-	-	-	0	10^{-3}	0	0.001	-	-
2	-	-	-	1	10^{-3}	0.135	4.173	0.016	0.050
3	1	4	1.2619	2	10^{-3}	0.116	5.922	0.026	0.069
4				3	10^{-3}	0.097	7.173	0.031	0.084
5				4	10^{-3}	0.097	7.795	0.034	0.091
6	2	5	1.4650	2	10^{-3}	0.107	6.504	0.028	0.076
7				3	10^{-3}	0.089	7.797	0.034	0.091
8				4	10^{-3}	0.089	8.327	0.037	0.097
9	3	6	1.6309	2	10^{-3}	0.110	7.237	0.032	0.084
10				3	10^{-3}	0.086	8.998	0.040	0.104
11				4	10^{-3}	0.085	9.795	0.044	0.113
12	4	7	1.7712	2	10^{-3}	0.101	7.275	0.032	0.084
13				3	10^{-3}	0.084	9.516	0.043	0.109
14				4	10^{-3}	0.082	10.117	0.045	0.114
15	5	8	1.8928	2	10^{-3}	0.106	7.571	0.034	0.087
16				3	10^{-3}	0.080	9.505	0.044	0.108
17				4	10^{-3}	0.078	10.216	0.047	0.116
18	1^M	4	1.2619	1	2.710	0.061	7.689	-	-
19	2^M	5	1.4650	1	2.959	0.054	8.671	-	-
20	3^M	6	1.6309	1	3.544	0.051	10.267	-	-
21	4^M	7	1.7712	1	3.662	0.046	10.653	-	-
22	5^M	8	1.8928	1	3.800	0.041	11.068	-	-
23	1	4	1.2619	2	10^{-3}	0.106	6.184	0.027	0.072
24				3	10^{-3}	0.094	7.361	0.032	0.086
25				4	10^{-3}	0.091	7.508	0.033	0.089
26	5	8	1.8928	2	10^{-3}	0.108	7.804	0.035	0.089
27				3	10^{-3}	0.085	10.135	0.047	0.115
28				4	10^{-3}	0.083	10.602	0.049	0.121
29	1	4	1.2619	1	10^{-3}	0.096	9.024	-	-
30	2	5	1.4650	1	10^{-3}	0.087	9.873	-	-
31	3	6	1.6309	1	10^{-3}	0.084	10.164	-	-
32	4	7	1.7712	1	10^{-3}	0.085	10.513	-	-
33	5	8	1.8928	1	10^{-3}	0.083	11.205	-	-

Table 1: Topographies used to determine $z_{0,\mathrm{Eff.}}$ and evaluate correlation parameters. Cases 1 to 17 are randomly distributed Sierpiński carpet, Cases 18 to 22 are Case 2, accompanied by a model for unresolved generations, Cases 23 to 28 are "pure" Sierpiński carpet templates (i.e., without the horizontal shift). Cases 29 to 33 are equivalent to Cases 5, 8, 11, 14, and 17, respectively, but the simulations run with relatively higher resolution (in order to assess resolution dependence). r is the scale-reduction ratio, N_b is the repeating factor (IFS input argument), D is the fractal dimension, N_g is the generation number, d/H and $z_{0,\mathrm{Eff.}}/H$ is zero-plane displacement height and effective aerodynamic roughness length, respectively, determined *a posteriori* and normalized by the flow depth. In addition, α and α_g are roughness model parameters outlined in Equation 4 and Section 3.1. *denotes multiplication by 10^3.

3. Results

This section is composed of two complementary parts. In the first part (Section 3.1), results of *a posteriori*-determined model parameters from Equation 4 are shown. We show that Equation 4 can reproduce the momentum deficit for unresolved generations, i.e., the "bulk" parameter exhibits striking similarity. In Section 3.2, we report vertical profiles of turbulence statistics. Averages are based upon many thousand large-eddy turnovers (a description of the LES code is not provided in this report, for brevity; the code has been summarized in numerous preceding articles). Note also that

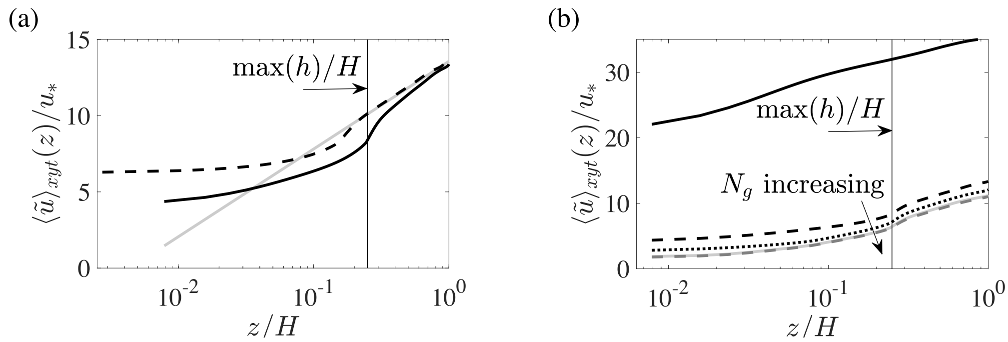

Figure 3: Vertical profiles of plane- and time-averaged streamwise velocity. Panel (a): Case 2 profile from LES (solid black), d-compensated velocity profile(dashed black), and logarithmic profile (solid gray). Panel (b): Case 1 (solid black), Case 2 (dashed black), Case 15 (dotted black), Case 16 (solid gray), and Case 17 (dashed gray). For reference, the maximum height of the topography is shown, $\max(h)/H$, which correlates closely with the inflection elevation; Panel (b) includes annotation for the direction of increasing N_g.

spatial (plane) averaging, $\langle \ldots \rangle_{xy}$, is performed on a “fluid averaging” basis; that is, the cumulative velocity at each level is divided only by the number of nodes occupied by fluid [19]. It is not instructive to show results for all cases in Table 1; instead, we have considered “limiting cases”, on the premise that turbulence statistics vary monotonically with intermediate topographic arrangements.

3.1. Parameter evaluation, model efficacy

Figure 3 shows vertical profiles of plane- and time-averaged streamwise velocity. Figure 3a shows the velocity profile for Case 2, before (solid black) and after (dashed black) correction for the displacement height, $d = \int_0^h z f_{b,x}(z) \mathrm{d}z / \int_0^h f_{b,x}(z) \mathrm{d}z$, where $f_{b,x}$ is the streamwise component of the body force imposed via IBM. For completeness, d/H is summarized in Table 1. With this, d/H is subtracted from elevation, z/H, to generate the dashed black line, and this profile is extrapolated to determine $z_{0,\mathrm{Eff.}}$ *a posteriori*. We remind the reader that spectral discretization in the horizontal directions renders all cases physically equivalent to flow over an infinitely-repeating array of blocks.

Figure 3b shows vertical profiles of plane- and time-averaged streamwise velocity for Case 1, Case 2, and Cases 15 to 17. Thus, for a given fractal dimension (in Figure 3b, $D = 1.8928$), the figure reveals how momentum penalty increases monotonically with number of generations, N_g. Due to the physics of the problem and the observation of diminishing influence of higher N_g, we find that a convergence may exist even with additional IFS iterations. This is due to the homogenization of additional blocks within the additional background roughness that is defined *a priori* within Equation 4 ($z_{0,p}$).

For Cases 2 to 17, Figure 4a shows α_g from Equation 4, determined *a posteriori* by fitting logarithmic profiles to the d-compensated plane- and time-averaged velocity profiles (for completeness, $z_{0,\mathrm{Eff.}}$ is summarized in Table 1). Annotation of the direction of increasing fractal dimension is also shown on Figure 4a. One can deduce that $\alpha_g = \alpha_g(N_g, D)$, although the N_g-dependence attenuates over the range considered. Physically, one can envision a scenario of “diminishing returns” with increasing N_g, to the extent that additional iterations will become homogenized with the “background” $z_{0,p}$ in Equation 4. Moreover, there are practical limitations on the requisite number of iterations, since natural urban topographies do not continue self-replicating *ad infinitum*. Note that the dependence and trends in $\alpha_g(N_g, D)$ are roughly equivalent for the “pure” and randomly-shifted fractal topographies (symbols denoted in Figure 4a caption).

Given the ostensible α_g tendency towards convergence at $N_g = 4$, beyond which $\alpha_g = \alpha_g(N_g, D) \rightarrow$

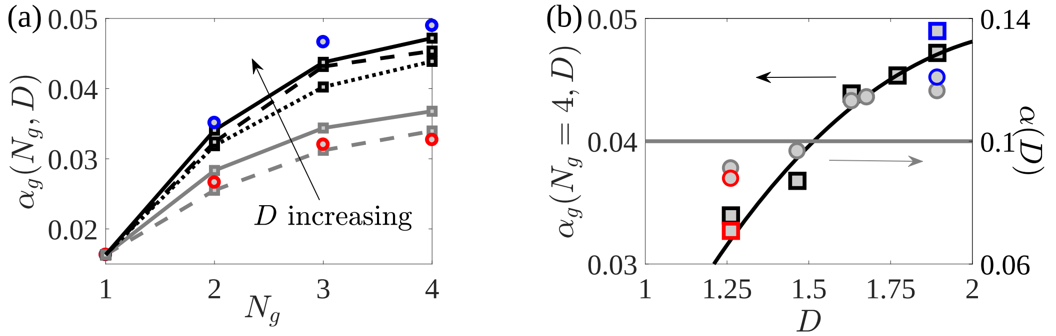

Figure 4: (Color) Equation 4 parameters. Panel (a) shows α_g with respect to N_g, for the five values of D considered (Series 1, 2, 3, 4, and 5 denoted by dashed gray line, solid gray line, dotted black line, dashed black line, and solid black line, respectively). The squares correspond with the randomly-shifted cases (Cases 2, 3-17), while the circles correspond with a "pure" Sierpiński carpet template, with red for Cases 23 to 25, and blue for Cases 26 to 28, respectively. Panel (b) shows the coefficient $\alpha_g(N_g = 4, D)$ (left ordinate, filled squares) and $\alpha = \alpha_g(N_g = 4, D)(1 + sk)^{\beta}$ (right ordinate, filled circles) with respect to fractal dimension. Red circle and square correspond with Case 25, blue circle and square correspond with Case 28.

$\alpha_g(D)$, we selected $\alpha_g(N_g = 4, D)$ as the "steady state" value. These values are summarized in Figure 4b, alongside the aggregate prefactor, $\alpha(D) = \alpha_g(N_g = 4, D)(1 + sk)^{\beta}$, in Equation 4. It is important to note that while $\alpha_g(N_g = 4, D) \sim D^2$ (solid black), $\alpha(D) \rightarrow \alpha \approx 10^{-1}$, as the D-dependence effectively vanishes; inclusion of the values for the "pure" and randomly-shifted Sierpiński carpet template reveals that the layout is essentially negligible. Note that either $\alpha = 10^{-1}$ or $\alpha_g(1 + sk)^{\beta}$ can be adopted for modeling unresolved generations.

It is worthwhile noting that $\alpha = 10^{-1}$ has a strong precedent [6]. Many prior studies — based on simulations, experiments, and field observations of the atmospheric surface layer, and in applications to a variety of dramatically-different rough boundaries — have reported $\alpha \approx 10^{-1}$. Although it is beyond the scope of this article to survey all preceding studies, we direct the interested reader to articles including Garratt [20], Zagarola and Smits [21], Tsai and Tsuang [22], Schultz and Flack [23], Flack and Schultz [16], Anderson and Meneveau [6], Anderson [24], Zhu et al. [13], and references therein. For completeness, $\alpha(D)$ and $\alpha_g(N_g, D)$ are summarized in Table 1.

The prognostic efficacy of the model can be readily assessed by considering a series of additional LES cases, wherein the Case 2 simulation is repeated, but the sub-generation roughness model is used where $h(x, y) = 0$, that is, $z_{0,p}$ in Equation 4 becomes $z_{0,p} \rightarrow \alpha_g(D)(1 + sk)^{\beta}\sigma_h^{\Delta}$, where σ_h^{Δ} is the root-mean-square associated with sub-generation iterations (i.e., $2 \leq N_g \leq 4$). In this sense, the aerodynamic loading associated with sub-generation scale iterations is imposed entirely through the equilibrium logarithmic law, and the approach is valid since the model parameters have been tuned *a priori* from the preceding exercise. For $D = 1.2619$, the results of this approach are shown in Figure 5, where the solid black and solid gray profiles correspond with Cases 2 and 5, respectively, where the velocity shift between the profiles is attributed to unresolved descendant generations.

When $z_{0,p} \rightarrow z_0$ (in Equation 4), however, the profiles for Case 5 and Case 18 (Case 2 with Equation 4 sub-generation model) collapse in the inertial layer; some deviation in the roughness sublayer, $z/H \lesssim \max(h)/H$, is guaranteed since actual elements are not being resolved. Although there are some differences in the roughness sublayer, they are confined to the lowest 10 % of the flow, and thus do not undermine the prognostic capabilities of the model. To further emphasize this, Figure 5 includes an inset for error,

$$\varepsilon(D) = \left\langle \left[\frac{[M(D, z_R) - O(D, z_R)]^2}{O(D, z_R)^2} \right]^{1/2} \right\rangle_{z_R}, \tag{5}$$

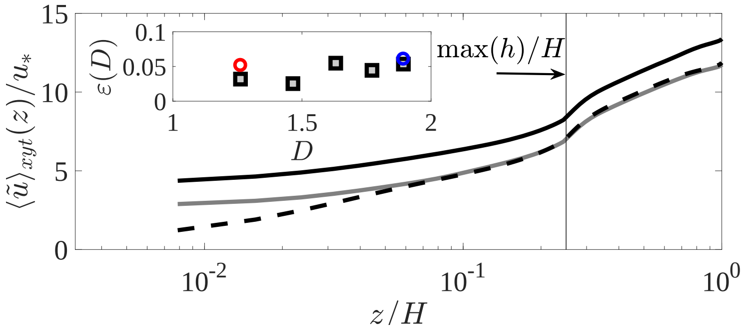

Figure 5: (Color) Vertical profile of plane- and time-averaged streamwise velocity for fully resolved Case 5 (solid gray), Case 2 without sub-generation model (solid black), and Case 18 (dashed black), which is identical to Case 2 but with sub-generation roughness model (Equation 4). Inset panel shows error, $\varepsilon(D)$, as per Equation 5 and accompanying text; squares correspond with randomly-shifted Sierpiński carpet templates, while red and blue symbols correspond with "pure" Sierpiński carpet template. Wall-normal position corresponding with maximum height, $\max(h)/H$, is shown for reference.

where $M(D, z_R) = \langle\tilde{u}\rangle_{xyt}(z_R)$ for Cases 18 to 22. $O(D, z_R) = \langle\tilde{u}\rangle_{xyt}(z_R)$ for Cases 5, 8, 11, 14, 17 (filled squares with black border), Case 25 (filled red circle), and Case 28 (filled blue circle) in the range $0.25 \leq z_R/H \leq 0.5$. Other ranges could have been used, but we found this sufficient to quantify differences between the modeled and actual cases. It is clear that $\varepsilon(D)$ is small, and insensitive to D. These errors are reasonable and, again, do not undermine the prognostic capabilities embodied in this approach.

The results presented in Figure 5 indicate that Equation 4 is a promising approach to the parameterization of small-scale, unresolved generations. The results also reveal that — in a first-order, plane- and time-averaged sense — the roughness model parameters are insensitive to the spatial layout of the underlying topography. However, these results do not illustrate how the dynamics of aloft mixing responds to the omission (or random spatial shift) of descendant generations. In Section 3.2, we address precisely this point via presentation of higher-order turbulence statistics.

3.2. Turbulence statistics and Sierpiński carpet templates

To assess the aerodynamic signature of the "pure" Sierpiński carpet template (Cases 23 to 28), the randomly-shifted Sierpiński template (Cases 3 to 17), and cases with models for unresolved sub-generations (Cases 18 to 22), we show vertical profiles of time- and plane-averaged first- to third-order turbulence statistics. We show only plane-averaged statistics, aware that spatial heterogeneities associated with emanating wakes, etc., may undermine the statistics. In results not shown here, we have assessed vertical profiles from virtual towers, and the results differ only within the canopy (i.e., for $z/\max(h) \lesssim 1$). This is due, mainly, to the overarching role played by the first generation (Case 2), where additional blocks appear to impart only a modest influence (at least as observed with the turbulence statistics considered here).

Figure 6 shows vertical profiles of time- and plane-averaged streamwise velocity for cases corresponding with the upper and lower limit of fractal dimension (Figure 6a: $D = 1.2619$; Figure 6b: $D = 1.8928$). The figures provide a means to assess: (1) how the outer (inertial) layer statistics respond to parameterized descendant generations; and (2) how the outer layer responds to the random spatial shift of successive generations, relative to the "pure" Sierpiński carpet template. There is generally very close agreement between the different profiles for $z/H \gtrsim 0.1$, which falls beneath the height of the large central block. This result is partially reflected in the Figure 5 inset, but the results in Figure 6 would also suggest that the choice of "pure" or randomly-shifted successive generations during IFS construction has negligible impact on the flow.

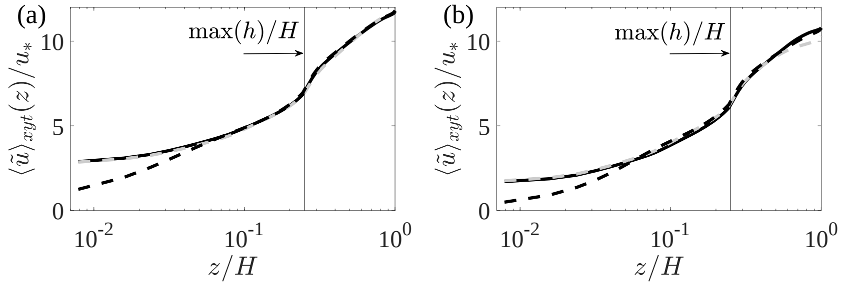

Figure 6: Assessing the impact of random spatial shifts in successive IFS generations. Vertical profiles of plane- and time-averaged streamwise velocity. On Panel (a), profiles correspond with Cases 5 (solid black), 18 (dashed black), and 25 (dashed gray). On Panel (b), profiles correspond with Cases 17 (solid black), 22 (dashed black), and 28 (dashed gray).

We present vertical profiles of Reynolds-averaged second- and third-order turbulence moments. Beginning firstly with vertical profiles of the total turbulent stresses:

$$\langle \boldsymbol{u}' \otimes \boldsymbol{u}' \rangle_t = \underbrace{\langle \tilde{\boldsymbol{u}}' \otimes \tilde{\boldsymbol{u}}' \rangle_t}_{\text{Resolved}} + \underbrace{\langle \boldsymbol{\tau} \rangle_t}_{\text{Subgrid}} \tag{6}$$

where $\langle \tilde{\boldsymbol{u}}' \otimes \tilde{\boldsymbol{u}}' \rangle_t$ and $\langle \boldsymbol{\tau} \rangle_t$ denote contributions to the total stresses as depicted by the underbraces [25]. Vertical profiles of the streamwise–wall-normal Reynolds stress, $\langle u'w' \rangle_{x,y,t}(z)$, are shown in Figure 7(a,e). In addition, we compute the contribution from Quadrants 1 to 4 events to the resolved streamwise–wall-normal turbulent stress based on,

$$\langle \tilde{u}'\tilde{w}' \rangle(\boldsymbol{x}, t; \mathcal{H})|_Q = \frac{1}{N_t} \sum_{j=1}^{N_t} \tilde{u}'(\boldsymbol{x}, t_j) \tilde{w}'(\boldsymbol{x}, t_j) I_Q(\boldsymbol{x}; \mathcal{H}), \tag{7}$$

where $\mathcal{H}$ is the so-called hole size and used to nominate a threshold on the magnitude of terms contributing to the turbulent stresses, N_t is the number of instants over which the conditional stress is to be recorded, and $I_Q(\boldsymbol{x}; \mathcal{H})$ is an indicator function used to isolate the role of different events based on their magnitude (or some predefined criteria):

$$I_Q(\boldsymbol{x}; \mathcal{H}) = \begin{cases} 1 & \text{if } |\tilde{u}'(\boldsymbol{x}, t)\tilde{w}'(\boldsymbol{x}, t)|_Q \geq T, \text{ and} \\ 0 & \text{if } |\tilde{u}'(\boldsymbol{x}, t)\tilde{w}'(\boldsymbol{x}, t)|_Q < T, \end{cases}$$

where $T = \mathcal{H} = 0$ in the present study, though alternative criteria can be used to define the threshold. For boundary layer turbulence, the ejection ($Q2$) and sweep ($Q4$) events are most relevant to the shear stress, while the contributions from $Q1$ and $Q3$ events are known to be rather modest [26]. Existing studies frequently report vertical profiles of the ratio of ejections to sweeps, i.e., $Q2/Q4$ [4, 19], and we adopt this approach and show the results in Figure 7(b,f).

Finally, in Figure 7(c,d,g,h), we show vertical profiles of skewness of resolved streamwise and vertical velocity fluctuation:

$$sk_{\tilde{u}'} = \frac{\langle (\tilde{u}')^3 \rangle_t}{\langle (\tilde{u}')^2 \rangle_t^{3/2}}, \qquad \text{and} \qquad sk_{\tilde{w}'} = \frac{\langle (\tilde{w}')^3 \rangle_t}{\langle (\tilde{w}')^2 \rangle_t^{3/2}}. \tag{8}$$

In the interest of generality, we show $\langle u'w' \rangle_t$, $Q2/Q4$, $sk_{\tilde{u}'}$, and $sk_{\tilde{w}'}$ for Cases with $D = 1.262$ (Figure 7a-d) and $D = 1.893$ (Figure 7e-h) – the upper and lower limit of fractal dimension considered in this article. In addition, we show results for the randomly-shifted Sierpiński templates, pure Sierpiński templates, cases with modeled descendant generations, and Case 2, which serves as a comparative benchmark (description of the figure profiles provided in caption).

A series of key deductions are made from inspection of Figure 7. First, note that for the modeled cases (Cases 18 and 22, both denoted by light gray on the panels), the domain includes only the first-generation block, while the *a posteriori*-determined roughness model parameters are used in Equation 1 to model the effects of descendant generations during LES. To this extent, Cases 18 and 22 are low-pass filtered versions of Cases 5 and 17 (dark gray on Figure 7 panels), respectively, while Cases 25 and 28 are "pure" Sierpiński carpet analogs of the fully-resolved, randomly-shifted cases.

Above the canopy, $z/\max(h) > 1$ (horizontal black line), the profiles all rapidly converge. This is especially true of the Reynolds stresses (Figure 7a,e), while effects of descendant blocks and/or block layout are slightly more persistent in other statistics. For all turbulence quantities, however, by $z/h \gtrsim 2$ the profiles are indistinguishable. Recall that Case 2 (red) is a central block, but spectral discretization in the horizontal directions renders this case equivalent to an infinitely-repeating array of large blocks. To this extent, the arrangement may be viewed as flow over an array of blocks, and thus the roughness sublayer will be occupied by a mixing layer-like structure (obstructed shear flow [27]). Other flow metrics (spectral density, for example), may reveal persistent flow perturbations over the depth of the domain [28], although such considerations are not the focus of this article.

It is certainly clear that differences emerge within the canopy, $z/h \lesssim 1$, although the differences are modest. Perhaps most striking are differences in $Q2/Q4$ (Figures 7b,f) and $sk_{\tilde{u}'}$ (Figure 7c,g) for $z/h \lesssim 1$. $Q2/Q4$ is larger for the benchmark (Case 2, red), indicating that sweeps contribute relatively less to the formation of Reynolds stresses. This can be readily understood via geometric considerations: Case 2 is an isolated block, and so the contribution from sweeps due to Kelvin-Helmholtz-like eddies in the roughness sublayer must be relatively weaker for this case since there are a lesser number of elements available to initiate their production. The result is also reflected in the skewness, where $\tilde{u}'$ exhibits a greater tendency towards negative values within the canopy. The vertical velocity skewness appears least sensitive to building layout.

The vertical profiles for $Q2/Q4$ (Figure 7b,f) and $sk_{\tilde{u}'}$ (Figure 7c,g) exhibit a distinct undulation beneath the elevation of the first block, $z/h \lesssim 1$. A substantial effort was dedicated to isolating the source of this undulation, since it was at first presumed to be a post-processing error. However, the undulation remained insensitive to differing averaging techniques: for the purpose of this article, plane averaging is used during LES to compute fluctuations, and the resultant turbulence quantities are time averaged *a posteriori*; we also loaded a Reynolds-averaged flow, $\langle \boldsymbol{u} \rangle_t$, and used this to accumulate fluctuations during LES, and the resultant turbulence quantities were indistinguishable to those attained with the former approach. In additional testing (results not shown here) to demonstrate that the undulation is a physical outcome associated with the urban topology considered – and not the LES code or averaging procedures – we have modeled flow over an urban arrangement considered previously by Coceal et al. [4]. They performed direct numerical simulation (DNS) of flow over an array of uniform height, staggered blocks, under inertial-dominated conditions (i.e., dynamic similarity exists between their DNS and our LES). The $Q2/Q4$ profiles, and the contribution to the resolved streamwise–wall-normal turbulent stresses from both, agree closely with the Coceal et al. [4] data.

Finally, it must be emphasized that the choice of building spatial template – pure or randomly-shifted Sierpiński – or the use of models for descendant generation, has a minimal influence on the inertial layer flow attributes (again, based on the turbulence statistics considered here).

4. Concluding remarks

Multiscale, fractal-like geometries are commonly encountered by the atmospheric surface layer, with urban topographies posing particular closure challenges owing to the disparate range of scales and dramatic aerodynamic signature. The research effort enabled via ARO Project # 65843-CH has addressed precisely this challenge. The PI and a supporting doctoral student have introduced a new closure for modeling aerodynamic drag – used previously for "engineering"-type flows, but capable

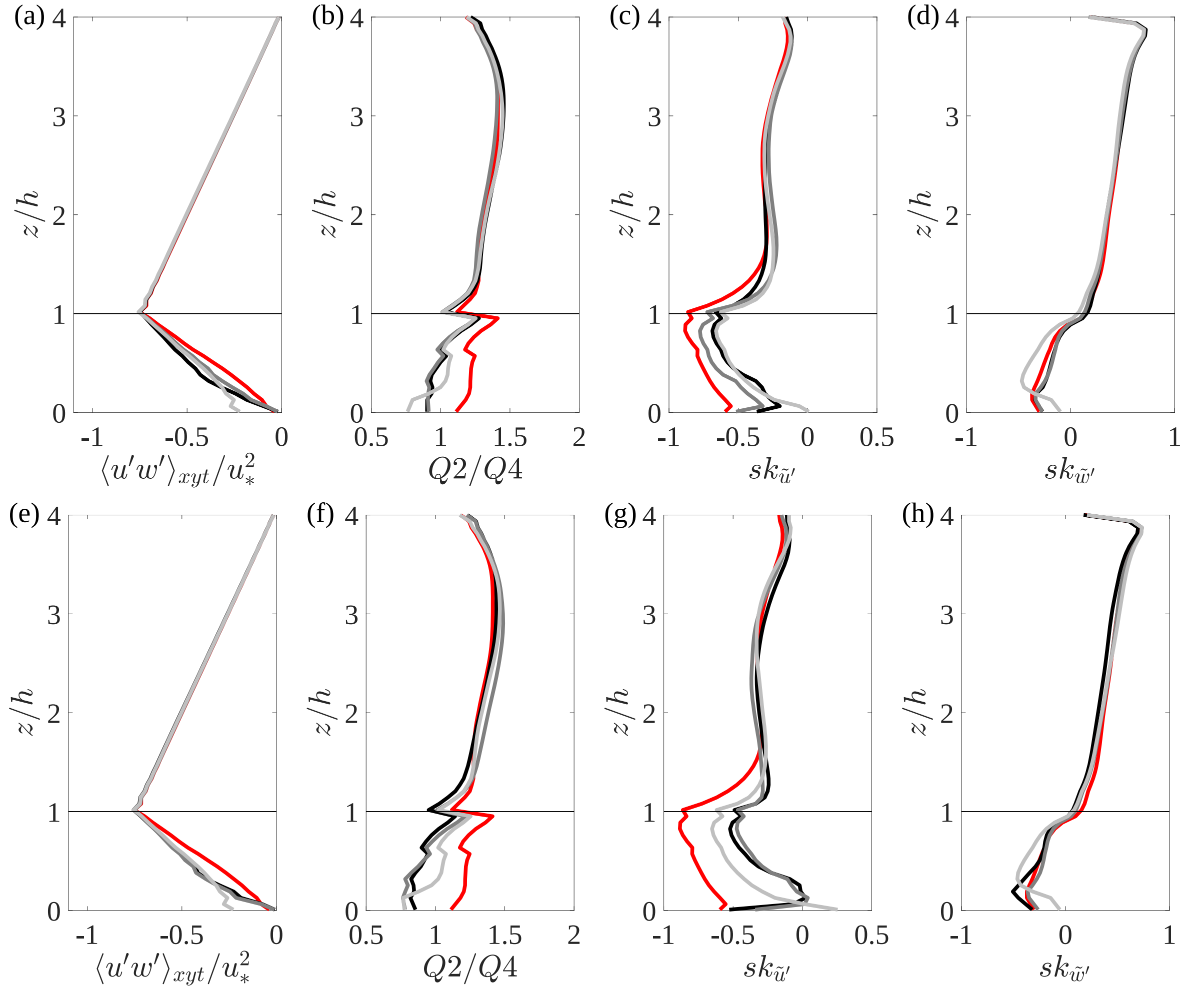

Figure 7: (Color) Vertical profiles of plane- and Reynolds-averaged turbulence statistics. Panels (a,e): streamwise–wall-normal Reynolds (total) stresses (Equation 6). Panels (b,f): ratio of contribution to production of resolved streamwise–wall-normal total stresses from sweeps, relative to ejections (Equations 7 and 3.2). Panels (c,g): skewness of resolved streamwise velocity (Equation 8). Panels (d,h): skewness of resolved vertical velocity (Equation 8). On Panels (a) to (d), line colors correspond with Case 25 (black), Case 5 (gray), Case 18 (light gray), and Case 2 (red); On Panels (e) to (h), line colors correspond with Case 28 (black), Case 17 (gray), Case 22 (light gray), and Case 2 (red).

of wider applicability – and have demonstrated excellent performance. In dissemination from this research effort, the investigative team have demonstrated strong performance of the model in a variety of contexts.

Towards the conclusion of the research effort, the PI and doctoral student turned attention to the additional challenge of scalar flux prescription – indeed, in urban micrometeorology, scalar fluxes have widespread importance – although unfortunately the project concluded before this work could be completed. With this, it is the opinion of the PI that additional work should focus on application of an Equation 4-style model, but for the application of scalar fluxes.

5. Doctoral Student: Travel Award and Princeton Visit

The research effort has been directed by PI Anderson, while a doctoral student, Xiaowei Zhu, has performed simulations and post-processing in support of the research effort. Xiaowei is reaching the end of his third year at UT Dallas, and will soon graduate from the program. He has been supported by the ARO throughout his tenure at UT Dallas. In addition to his scholarly activities, this student received a UT Dallas travel award in 2016. This award not only reflects university support for this ARO project, but it also provided Xiaowei with another travel opportunity (beyond attendance at conferences). The travel award funds were used to send Xiaowei for a one-week visit to Princeton University, where he worked with collaborator, Elie Bou-Zied. At Princeton, Xiaowei gained experience with modeling flows over heated cubes – resembling daytime conditions in the urban roughness sublayer. This is a new capability for the group, and it addresses a long-term interest on the need prognostic scalar roughness length models in flows over complex, multiscale environments [29]. As noted in the preceding section, this research will be the topic of our Year # 3 research effort.

6. Dissemination

The work described above (from Years # 1 and 2 of the research effort) has been presented through a series of invited seminars, conference talks/proceedings, peer-review publications, and outreach activities. The below summarizes dissemination of research during the research effort.

Invited Talks:

- November, 2018: Center for Astrophysics, Space Physics, and Engineering Research, Baylor University, Waco, Texas.
- October, 2018: Department of Mechanical Engineering, University of Houston, Houston, Texas.
- July, 2018: Invited Speaker in session "Scale-Resolving Turbulence Simulation", World Congress on Computational Mechanics, New York, NY.
- June, 2018: Kavli Institute for Theoretical Physics, University of California at Santa Barbara – invited speaker in program "Planetary Boundary Layers in Atmospheres, Oceans, and Ice on Earth and Moons".
- May, 2018: Department of Mechanical Engineering, Queensland University of Technology, Brisbane, Australia.
- May, 2018: Department of Mechanical Engineering, Monash University, Melbourne, Australia.
- May, 2018: Department of Mechanical Engineering, The University of Melbourne, Melbourne, Australia.
- May, 2018: Department of Mechanical Engineering, Monash University, Melbourne, Australia.
- March, 2018: Invited Seminar, Department of Mechanical and Aerospace Engineering, Arizona State University, Tempe, Arizona.
- November, 2017: Guest lecture, "Turbulence modeling with large-eddy simulation", Southern Methodist University, Dallas, Texas.
- November, 2017: Invited Speaker at Joint Workshop of Mathematicians, Biogeochemists and Atmospheric Scientists, Helsinki, Finland.
- November, 2017: Invited Seminar at Southwest Research Institute, University of Colorado at Boulder, Denver, Colorado.
- September, 2017: Invited Speaker at Symposium on Meteorology and Climate – Modeling for Air Quality, Davis, California.
- May, 2017: Department of Mechanical Engineering, The University of Utah.
- June, 2017: Invited Speaker at Engineering Mechanics Institute (EMI) Conference, University of California at San Diego, San Diego, Calif.
- May, 2017: School of Environment and Society, Tokyo Institute of Technology, Tokyo, Japan.

- April, 2017: *Graduate Seminar Series, Department of Mechanical and Aerospace Engineering, University of Texas at Arlington*, Arlington, TX.
- April, 2017: *Graduate school and fluid mechanics. Dallas County Community College District, STEM Foundation, "STEM Summit"*, Dallas, TX.
- October, 2016: *Perot Museum, Social Sciences Evening*, "Fluid flows in engineering and the environment: math, mystery ... and a few anecdotes", Dallas, TX.
- September, 2016: *Departmental Seminar Series, Department of Mechanical Engineering, University of Texas at Dallas*, Dallas, TX.
- October, 2016: *Departmental Seminar Series, Department of Mechanical Engineering, University of Texas at Dallas*, Dallas, TX.

Conference Proceedings:

*ARO-supported graduate student; $^+$ARO-supported post-doctoral scholar; †Presenting author

- Oral presentation: Zhu X*,†, **Anderson W**, 2018: Proceedings of American Physical Society, Division of Fluid Dynamics, Atlanta, Georgia.
- Oral presentation: Zhu X*,†, **Anderson W**, 2018: Proceedings of the American Meteorological Society, Symposium on Boundary Layers and Turbulence, Oklahoma City, OK.
- Oral presentation: Zhu X*, **Anderson W**†, 2018: Proceedings of the 8th International Symposium on Environmental Hydraulics, South Bend, IN.
- Oral presentation: Zhu X*,†, Anderson W, 2017: Proceedings of American Physical Society, Division of Fluid Dynamics, Denver, Colorado.
- Oral presentation: Zhu X*,†, Anderson W, 2017: Proceedings of Bluebonnet Symposium on Thermal-Fluid Sciences, Dallas, Texas.
- Oral presentation: Zhu X*,†, **Anderson W**, 2016: Proceedings of American Physical Society, Annual Meeting of the Division of Fluid Dynamics, Portland, OR.
- Oral presentation: Zhu X*,†, **Anderson W**, 2016: Proceedings of American Meteorological Society, Symposium on Boundary Layers and Turbulence, Salt Lake City, UT.
- Oral presentation: Li Q†, Bou-Zeid E, Anderson W, 2016: Proceedings of American Meteorological Society, Symposium on Boundary Layers and Turbulence, Salt Lake City, UT.

Outreach:

- April, 2017: *Graduate school and fluid mechanics. Dallas County Community College District, STEM Foundation, "STEM Summit"*, Dallas, TX.
- October, 2016: *Perot Museum, Social Sciences Evening*, "Fluid flows in engineering and the environment: math, mystery ... and a few anecdotes", Dallas, TX.

Peer-Review Journal:

*ARO-supported graduate student; †Corresponding author

- Li Q, Bou-Zeid E†, **Anderson W**, Grimmond S, Hultmark M, 2016: Quality and reliability of LES of convective scalar transfer at high Reynolds numbers. *International Journal of Heat and Mass Transport* **102**, 959—970 [30].
- Zhu X$^+$, Iungo V, Leonardi S, **Anderson W**†, 2016: Large-eddy simulation study of urban-like topography statistical moments relevant to setting roughness length via *a priori* models. *Boundary-Layer Meteorology* doi:10.1007/s10546-016-0198-x [13].

- Li Q, Bou-Zeid E†, **Anderson W**, 2016: The impact and treatment of the Gibbs phenomenon in immersed boundary method simulations of momentum and scalar transport. *Journal of Computational Physics* **310**, 237-251 [31].
- Zhu X^{+}, **Anderson W**†, 2018: Numerical simulation of turbulent flow over urban-like fractal topographies: prognostic models for unresolved momentum fluxes. *Journal of Turbulence "In Revision"* [32].

7. Mentoring

Grant # W911NF-15-1-0231 supported UT Dallas doctoral candidate, Xiaowei Zhu. Xiaowei joined the PI at UT Dallas in Fall, 2014, and completed three years of doctoral research under the PI's supervision. He graduated in August, 2018, at the end of Project # 65843-CH. This was the PI's first graduated doctoral student. This student has presented his research at numerous conferences, and is first author of two peer-review articles (one published in *Boundary-Layer Meteorology*, the second was submitted to the *Journal of Turbulence*, and we are currently revising the article based on reviewer critiques; see also Section 6). Following graduation from UT Dallas, Xiaowei moved to Mechanical Engineering Department at The Johns Hopkins University, where is a post-doctoral scholar.

References Cited

[1] J.C. Wyngaard. *Turbulence in the Atmosphere.* Cambridge University Press, USA, 2010.

[2] H. Tennekes and J.L. Lumley. *A First Course in Turbulence.* MIT Press, Cambridge, MA, 1972.

[3] P.S. Jackson. On the displacement height in the logarithmic profile. *J. Fluid Mech.*, 111:15–25, 1981.

[4] O. Coceal, A. Dobre, T. G. Thomas, and S. E. Belcher. Structure of turbulent flow over regular arrays of cubical roughness. *J Fluid Mech*, 589:375–409, 2007.

[5] I. Rodriguez-Iturbe and A. Rinaldo. Fractal river basins: chance and self-organization. *Cambridge University Press, Cambridge*, 1997.

[6] W. Anderson and C. Meneveau. A dynamic large-eddy simulation model for boundary layer flow over multiscale, fractal-like surfaces. *J. Fluid Mech.*, 679:288–314, 2011.

[7] S. Chester, C. Meneveau, and M.B. Parlange. Modelling of turbulent flow over fractal trees with renormalized numerical simulation. *J. Comput. Phys.*, 225:427–448, 2007.

[8] Sara Encarnacao, Marcos Gaudiano, Francisco C. Santos, Jose A. Tenedorio, and Jorge M. Pacheco. Fractal cartography of urban areas. *Scientific Reports*, page DOI: 10.1038/srep00527, 2012.

[9] D. Queiros-Conde and J.C. Vassilicos. Turbulent wakes of 3d fractal grids (intermittency in turbulent flows). *Cambridge University Press, Cambridge*, 2001.

[10] R.E. Seoud and J.C. Vassilicos. Dissipation and decay of fractal-generated turbulence. *Phys. Fluids*, 19:105108, 2007.

[11] P.P. Sullivan and E.G. Patton. The effect of mesh resolution on convective boundary layer statistics and structures generated by large-eddy simulation. *J. Atmos. Sci.*, 68:2395–2415, 2011.

[12] E.G. Patton, P.P. Sullivan, R.H. Shaw, J.J. Finnigan, and J.C. Weil. Atmospheric stability influences on coupled boundary layer and canopy turbulence. *J. Atmos. Sci.*, 73:1621–1647, 2016.

[13] X. Zhu, V. Iungo, S Leonardi, and W. Anderson. Large-eddy simulation study of urban-like topography statistical moments relevant to setting roughness length: *a priori* models. *Boundary-Layer Meteorol.*, doi:10.1007/s10546-016-0183-4, 2016.

[14] R.W. Macdonald, R.F. Griffiths, and D.J. Hall. An improved method for the estimation of surface roughness of obstacle arrays. *Atmospheric Environment*, 32(11):1857–1864, 1998.

[15] Vincenzo Armenio, Bernard Geurts, and Jochen Fröhlich. *Direct and Large-eddy Simulation VII: Proceedings of the Seventh International ERCOFTAC Workshop on Direct and Large-Eddy Simulation, Held at the University of Trieste, September 8-10, 2008*, volume 13. Springer Science & Business Media, 2010.

[16] K.A. Flack and M.P. Schultz. Review of hydraulic roughness scales in the fully rough regime. *J. Fluids Eng.*, 132(4):041203, 2010.

[17] T. Ito, A. Matsumoto, T. Ito, M. Motozawa, K. Iwamoto, H. Kawashima, H. Ando, T. Senda, and Y. Kawaguchi. Experimental investigation on effects of surface roughness geometry affecting to flow resistance. In *ASME-JSME-KSME 2011 Joint Fluids Engineering Conference*, pages 3945–3954. American Society of Mechanical Engineers, 2011.

[18] H.-0. Peitgen, H. Jurgens, and D. Saupe. Chaos and fractals: New frontiers of science. *Springer-Verlag*, 1992.

[19] W. Anderson and M. Chamecki. Numerical study of turbulent flow over complex aeolian dune fields: The white sands national monument. *Phys. Rev. E*, 89:013005–1–14, 2014.

[20] J.R. Garratt. *The atmospheric boundary layer*. Cambridge University Press, 1994.

[21] M.V. Zagarola and A.J. Smits. Mean-flow scaling of turbulent pipe flow. *J Fluid Mech*, 373:33–79, 1998.

[22] J.-L. Tsai and B.-J. Tsuang. Aerodynamic roughness over an urban area and over two farmlands in a populated area as determined by wind profiles and surface energy flux measurements. *Agric. For. Meteorol.*, 132:154–170, 2005.

[23] M.P. Schultz and K.A. Flack. Turbulent boundary layers on a systematically varied rough wall. *Phys Fluids*, 21(1):015104, 2009.

[24] W. Anderson. An immersed boundary method wall model for high-reynolds number channel flow over complex topography. *Int. J. Numer. Methods Fluids*, 71:1588–1608, 2012.

[25] Stephen B Pope. *Turbulent flows*. Cambridge university press, 2000.

[26] R. Mejia-Alvarez and K.T. Christensen. Low-order representations of irregular surface roughness and their impact on a turbulent boundary layer. *Phys. Fluids*, 22:015106, 2010.

[27] M. Ghisalberti. Obstructed shear flows: similarities across systems and scales. *J Fluid Mech*, 641:51, 2009.

[28] J. Hong, J. Katz, and M. Schultz. Near-wall turbulence statistics and flow structures over three-dimensional roughness in a turbulent channel flow. *J. Fluid Mech.*, 667:1–37, 2011.

[29] W. Anderson. Passive scalar roughness lengths for atmospheric boundary layer flow over complex, fractal topographies. *Environmental Fluid Mechanics*, 13(5):479–501, 2013.

[30] Q. Li, E. Bou-Zeid, W. Anderson, S. Grimmond, and M. Hultmark. Quality and reliability of les of convective scalar transfer at high reynolds numbers. *Int. J. Heat Mass Trans.*, 102:959–970, 2016.

[31] Q. Li, E. Bou-Zeid, and W. Anderson. The impact and treatment of the gibbs phenomenon in immersed boundary method simulations of momentum and scalar transport. *J Comput Phys*, 310:237–251, 2016.

[32] X. Zhu and W. Anderson. Numerical simulation of turbulent flow over urban-like fractal topographies: prognostic models for unresolved momentum fluxes. *J. Turbulence, "In Revision"*, 2018.